

Nd- and Eu-Doped Cobalt Oxide Nanocrystals as Highly Efficient Electrocatalysts for Alkaline Water Splitting

Mehdi Salehi^{a,*}, Rahele Abdoos^b, Bahram Bahramian^b

^aDepartment of Chemistry, Semnan University, Semnan 35351-19111, Iran.

^bDepartment of Chemistry, Shahrood University

Article history:

Received: 26/Nov/2017

Received in revised form: 27/Dec/2017

Accepted: 29/Dec/2017

Abstract

In this study, characterization of Co_3O_4 nanoparticle and Nd and Eu doped on the cobalt oxide were presented. These nanoparticles were prepared by a combustion synthesis method for 8 h in the temperature 700°C using only complex $\text{Co}(\text{acac})_3$. Nanoparticles were characterized by infrared spectroscopy (IR), X-ray diffraction (XRD), scanning electron microscopy (SEM), elemental maps analysis, energy-dispersive X-ray spectroscopy (EDS) and diffuse reflectance spectroscopy (DRS). The effect of neodymium and europium additive was also studied using cyclic voltammetry (CV) for the oxygen evolution reaction in an alkaline environment. Analysis of electrocatalytic activity for oxygen evolution reaction (OER) demonstrated that eridium efficiency increases the current of the oxygen evolution. Meanwhile, neodymium has no effect on the properties of Co_3O_4 in this case.

Keywords: Cobalt oxide; (Co_3O_4) nanoparticles; Combustion synthesis; Electrocatalytic activity.

1. Introduction

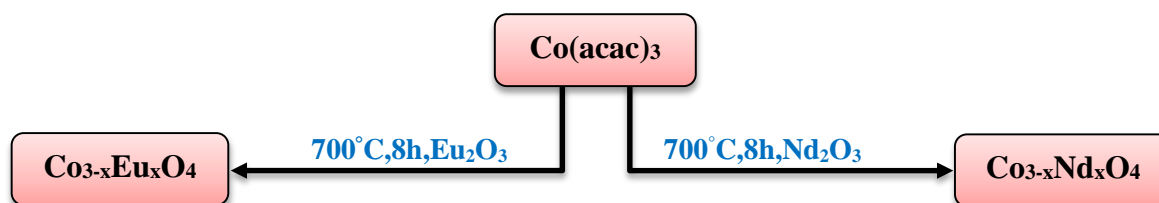
In recent years cobalt oxide (Co_3O_4) nanoparticles as a kind of functional material that different shapes have been synthesized including nanofibers, nanorods, nanocubes, nanoboxes, nanowires, nanodisks, nanotubes and hollow nanospheres [1-9]. Different methods for the synthesis of nanoparticles have been reported such as chemical spray pyrolysis [10], chemical vapour deposition [11], sol-gel method [12], reduction-oxidation routes [13], gel hydrothermal oxidation [14], cobalt salt decomposition [15-17] and solvothermal decomposition [18]. The present work investigates the Combustion synthesis of cobalt oxide doped Neodymium oxide ($\text{Co}_{3-x}\text{Nd}_x\text{O}_4$) and Europium oxide ($\text{Co}_{3-x}\text{Eu}_x\text{O}_4$).

The applications of Co_3O_4 nanoparticles including catalysis [19-21], solid state sensors [22-23] [24], electrochromic sensors [25], magnetism [26], and energy storage [27]. Co_3O_4 nanomaterials are used as a lithium battery through supercapacitors [28-30] and also as a black ceramic pigment [31-32]. In recent years, there has been a growing interest in cubic Co_3O_4 . Given that the Co_3O_4 have spinel structure of AB_2O_4 type (Co^{2+} cations occupy the tetrahedral sites and Co^{3+} cations occupy the octahedral sites in the crystal lattice.) [33]. Different materials are available for the production of these nanoparticles. Ranging from ceramic dielectrics [34], semiconductors [35], metals [36], and metal oxides [37-38].

* **Corresponding Author:** Department of Chemistry, Faculty of Sciences, University of semnan, Iran. E-mail: msalehi@semnan.ac.ir

New research has shown that metal oxides is very important due to their special properties and envisioned applications [39-40].

In this paper, we present a detailed study of cobalt-oxides nanoparticles and synthesis Co_3O_4 nanoparticles by a simple combustion synthesis method (scheme 1).



Scheme 1. Schematic illustration of the synthesis mechanism of Co_3O_4 and $\text{Co}_{3-x}\text{Nd}_x\text{O}_4$, $\text{Co}_{3-x}\text{Eu}_x\text{O}_4$ nanoparticles.

2. Experimental section

2.1. Materials and Product characteristics

All chemicals and solvents obtained from commercial sources (Merck Company) and were used without further purification. The materials being used in this work are: cobalt (II) Acetate, acetylacetone, hydrogen peroxide, Nd_2O_3 , Eu_2O_3 .

The morphology and composition of the Co_3O_4 nanoparticles were characterized with the Hitachi FESEM model S-4160 field emission scanning electron microscope (FESEM). Powder X-ray diffraction (XRD) data was collected with Cu-K α radiation in the 2θ range of $10-90^\circ$. FT-IR spectra were obtained in the wavelength range $400-4000\text{ cm}^{-1}$ with KBr pellet technique (measured by a FT-IR SHIMADZU spectrophotometer) Diffuse reflectance spectra (DRS) were collected with a V-670, JASCO spectrophotometer and transformed to the absorption spectra.

2.2. Synthesis of $\text{Co}(\text{acac})_3$

Optical resolution of $[\text{M}(\text{acac})_3]$ complexes have attracted considerable interest over the years. for synthesis $[\text{Co}(\text{acac})_3]$ complex (0.38 g) of cobalt(II) Acetate was dissolved in to 5 ml of distilled water (was stirred and heated to a temperature of 90 degrees) and then 5 ml acetylacetone was added with using a dropping pipette 4.5 mL of a 10% hydrogen peroxide solution was added to the mixture during 20 minutes. After 15 minutes with continuous stirring, the mixture was cooled in an ice water bath for 30 minutes. Dark green product created and filtered under vacuum and

then dry for 15 minutes in an oven at 100°C . Yield: 75%.

2.3. Synthesis of $\text{Co}_{3-x}\text{Nd}_x\text{O}_4$ and $\text{Co}_{3-x}\text{Eu}_x\text{O}_4$ nanoparticles

Appropriate molar amounts of $[\text{Co}(\text{acac})_3]$ and 0.01, 0.03 and 0.05 of Nd_2O_3 and Eu_2O_3 was added to the crucible containing amounts and in furnace was at 700°C for 8 hours. Nanoparticles of $\text{Co}_{3-x}\text{Nd}_x\text{O}_4$ and $\text{Co}_{3-x}\text{Eu}_x\text{O}_4$ were synthesized under these conditions.

2.4. Preparation of the electrodes

To prepare the electrodes for oxygen evolution reaction (OER), The GCE was polished mechanically with $5\ \mu\text{m}$ alumina slurry on a polishing cloth. then, the electrode was washed ultrasonically in a mixture of ethanol/distilled water solution (1:1 V/V) for 10 min and dried in the room temperature. To deposit Co_3O_4 and $\text{Co}_{2.97}\text{Nd}_{0.03}\text{O}_4$ and $\text{Co}_{2.97}\text{Eu}_{0.03}\text{O}_4$ on the electrode, 0.10 mg of the synthesized powders in 10 mL distilled water, $5.0\ \mu\text{L}$ of the suspension, Finally, $5\ \mu\text{L}$ of 1% wt. Nafion solution was dropped onto the electrode to increase the adhesion of the coatings to the surface, were mixed and then dried in air to prevent sample detachment from the working electrode during testing. The $\text{Co}_3\text{O}_4/\text{GCE}$, $\text{Co}_{2.97}\text{Nd}_{0.03}\text{O}_4/\text{GCE}$ and $\text{Co}_{2.97}\text{Eu}_{0.03}\text{O}_4/\text{GCE}$, were obtained using the above mentioned procedure.

3. Results and discussion

3.1. FTIR spectra

Infrared spectra (FTIR) of calcined samples were recorded in a FT-IR SHIMADZU spectrometer in the region of 4000–400 cm^{-1} .

Fig 1 a-c shows the FTIR spectra for the indicated Co_3O_4 nanoparticles (a), $(\text{Co}_{3-x}\text{Nd}_x\text{O}_4)$ (b) and

$(\text{Co}_{3-x}\text{Eu}_x\text{O}_4)$ (c) At 700°C. Studying Co_3O_4 nanoparticles by FT-IR, display two distinct bands at 576 (ν_1) and 665 (ν_2) cm^{-1} which emanate from the stretching vibrations of the M-O bonds, and they confirm the formation of Co_3O_4 spinel oxide [41–43]. The ν_1 band is characteristic of Co^{3+} vibration in the octahedral hole, and ν_2 band is attributable to Co^{2+} vibration in tetrahedral hole in the spinel lattice [44].

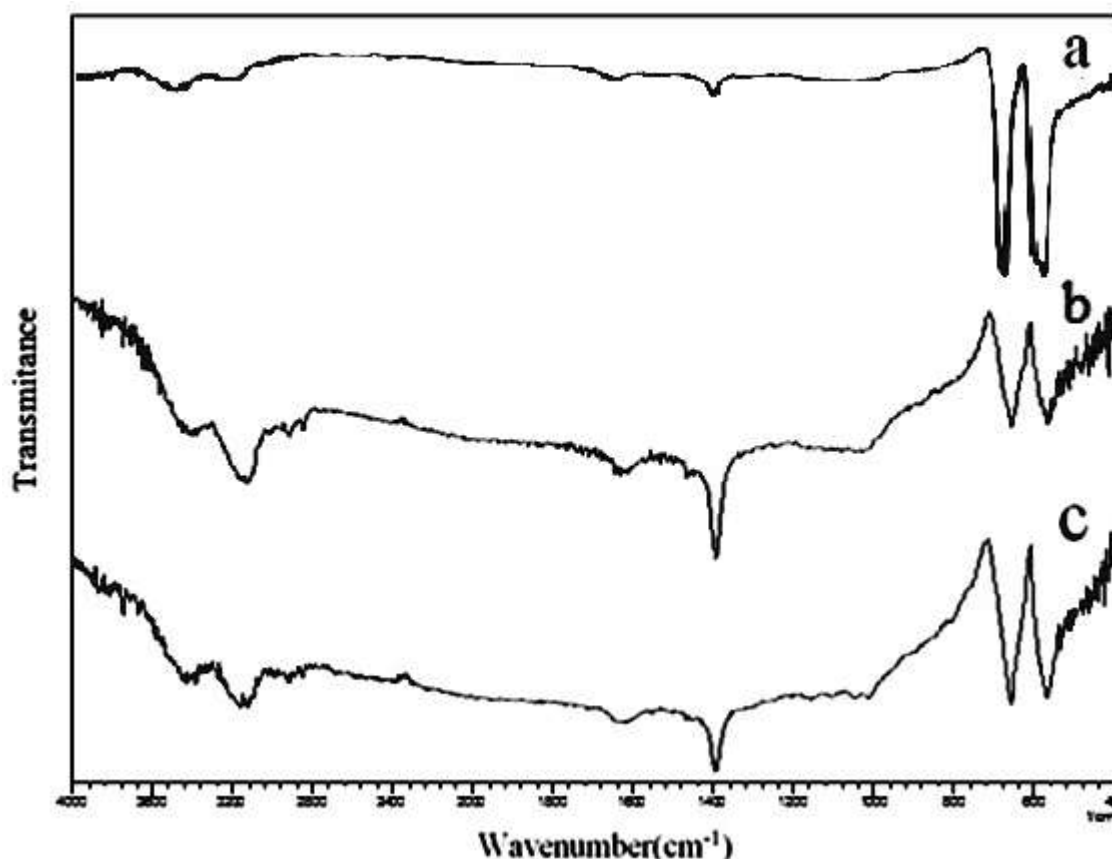


Fig. 1. FTIR spectrum of synthesized Co_3O_4 (a), $\text{Co}_{3-x}\text{Nd}_x\text{O}_4$ (b) and $\text{Co}_{3-x}\text{Eu}_x\text{O}_4$ (c) at 700°C nanoparticles.

3.2. Powder x-ray diffraction (XRD)

The crystallographic information of the two samples studied in $\text{Co}_{3-x}\text{Nd}_x\text{O}_4$ and $\text{Co}_{3-x}\text{Eu}_x\text{O}_4$ (0.0, 0.01, 0.03 and 0.05 mmol) was obtained with the X-ray powder diffraction (XRD).

Figure 2 show the powder X-ray diffraction (PXRD) patterns of the cobalt oxide nanoparticles prepared via Combustion synthesis from $\text{Co}(\text{acac})_3$ complex at temperature 700 °C for 8h.

Diffraction lines detected at $2\theta = 19.0^\circ$, 31.2° , 36.5° , 38.4° , 44.8° , 55.6° , 59.0° and 65.2° , in XRD patterns of the sample Co_3O_4 powder are assigned to the reflection (1 1 1), (2 0 0), (3 1 1), (2 2 2), (4 0 0), (4 2 2), (5 1 1)

and (4 4 0), respectively. These diffraction peaks correspond to the spinel cubic structure of Co_3O_4 with $\text{Fd}3\text{m}$ space group. Lattice parameters of cubic structure $a = b = c = 8.084 \text{ \AA}$. No peaks of any other phases or impurities were detected; indicating the high purity of the Co_3O_4 product. (JCPDS Card No. 43-1003).

Using the Sherrer formula for the calculation of particle sizes $D = 0.9\lambda/\beta \cos\theta$ where D is the average grain size, λ is the X-ray wavelength and θ is the angle of diffraction and β is the full width at half maximum of the strongest peak [45-48]

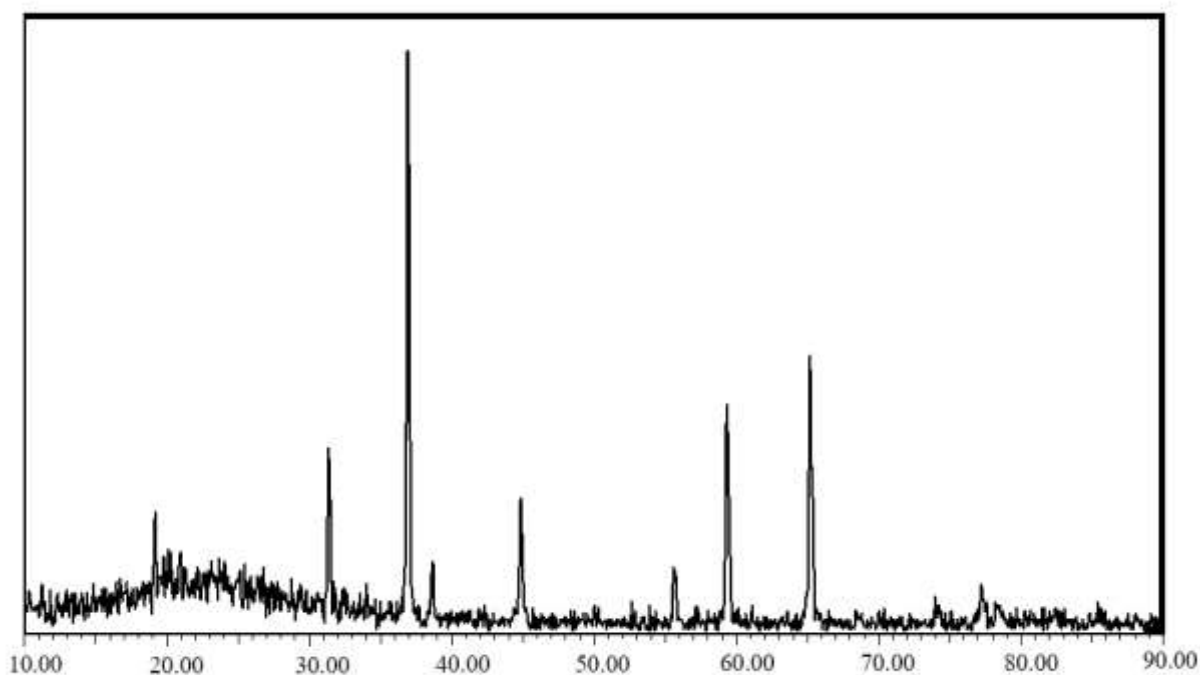


Fig. 2. X-ray powder diffraction pattern of the Co_3O_4 nanoparticles.

Figure 3 and 4 shows the XRD patterns of $\text{Co}_{3-x}\text{Nd}_x\text{O}_4$ and $\text{Co}_{3-x}\text{Eu}_x\text{O}_4$ in different mmol amounts of Nd and Eu ($x = 0.01, 0.03$ and 0.05 mmol) and comparison of them with pure Co_3O_4 .

With the increasing the amount of Nd^{3+} and Eu^{3+} , from $x = 0.01$ to 0.03 , no additional XRD lines pertaining to any secondary phase were observed so it is believed

that Nd^{3+} and Eu^{3+} does replace Co^{3+} . By increasing amount of Nd^{3+} and Eu^{3+} to 0.05 , an additional peak at $2\theta = 61.8^\circ$ for $\text{Co}_{3-x}\text{Nd}_x\text{O}_4$ and $2\theta = 47.3^\circ$ for $\text{Co}_{3-x}\text{Eu}_x\text{O}_4$ was observed which can be attributed to the excess of the Nd^{3+} and Eu^{3+} ions which have resided on the surface or on the grain boundaries of the nanocrystals. Thus, the maximum amount of doped is 0.03 mmol.

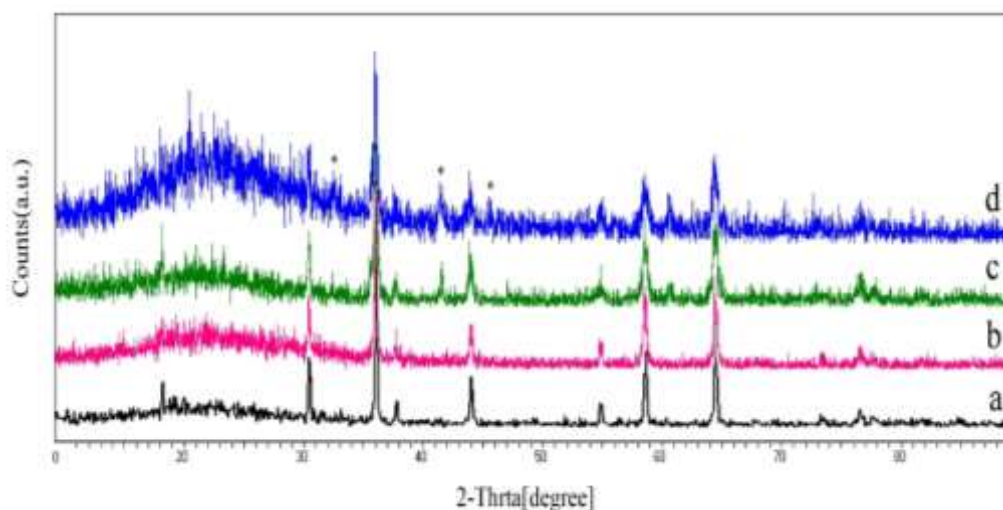


Fig. 3. PXRD patterns of the synthesized $\text{Co}_{3-x}\text{Nd}_x\text{O}_4$ nanoparticles, that a is pure Co_3O_4 , b is $x=0.01$, c is $x=0.03$, d is $x=0.05$. * is due to Nd_2O_3 impurity.

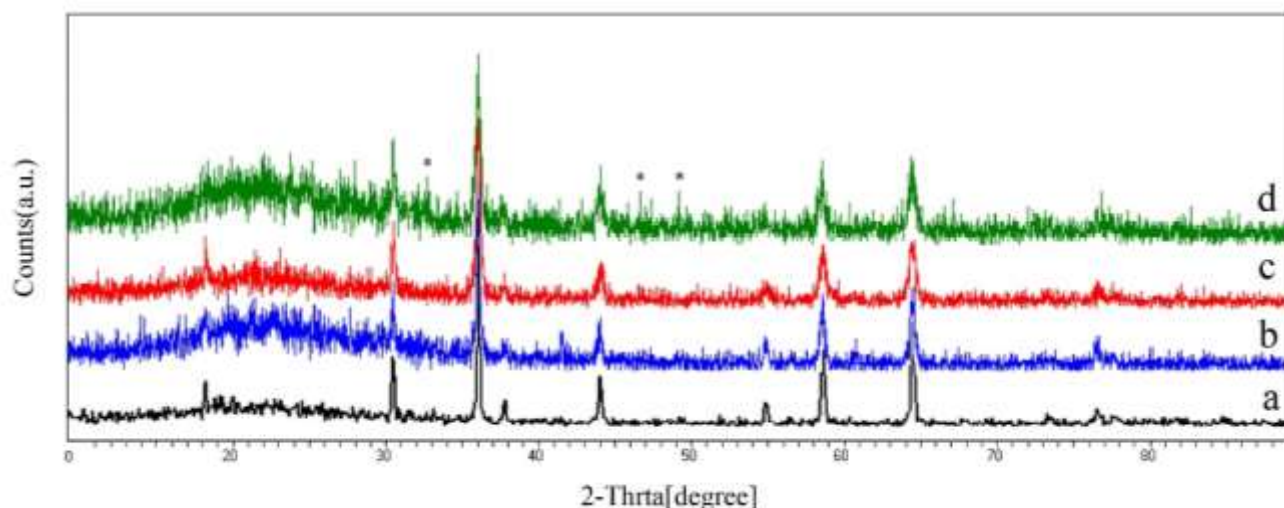


Fig. 4. XRD patterns of the synthesized $\text{Co}_{3-x}\text{Eu}_x\text{O}_4$ nanoparticles, that a is pure Co_3O_4 , b is $x=0.01$, c is $x=0.03$, d is $x=0.05$. * is due to Eu_2O_3 impurity

Table 1 shows the cell parameter refinement data for the pure and doped nanomaterials. With increasing the dopant amount, the parameter a, b and c have not changed. The obtained data confirmed the synthesis of Co_3O_4 , $\text{Co}_{3-x}\text{Nd}_x\text{O}_4$ and $\text{Co}_{3-x}\text{Eu}_x\text{O}_4$ confirmed Cubic phase spinel structure with lattice parameters of $a = b = c = 8.084 \text{ \AA}$. Thus unit cell size remain unchanged.

According to these images, SEM analysis revealed nearly uniform nanoparticles. It seems that the

Table 1. Cell parameter refinement data for the samples.

	Pure Co_3O_4	1 mmol of Nd^{3+}	3mmol of Nd^{3+}	5mmol of Nd^{3+}	1mmol of Eu^{3+}	3 mmol of Eu^{3+}	5mmol of Eu^{3+}
$a = b = c(\text{\AA})$	8.084	8.084	8.084	8.084	8.084	8.084	8.084
$2 \text{ Theta } (^{\circ})$	37.024	36.886	36.817	36.818	36.886	36.817	36.818

3.3. Morphological investigation

SEM images of spinel Co_3O_4 present in Fig. 5. Each nanoparticle takes on a spherical shape. a few number of voids is also observed on the surface of Co_3O_4 . Fig 6-8 shows the FESEM images of the Nd^{3+} and Fig 9-11 shows the FESEM images of the Eu^{3+} doped Co_3O_4 ($x = 0.01, 0.03$ and 0.05 molar ratio, respectively).

nanoparticles are size-homogeneous with an average particle size of around 40-50 nm. It is obvious that the morphology of $\text{Co}_{3-x}\text{Nd}_x\text{O}_4$ and $\text{Co}_{3-x}\text{Eu}_x\text{O}_4$ higher uniformity compared to undoped sample

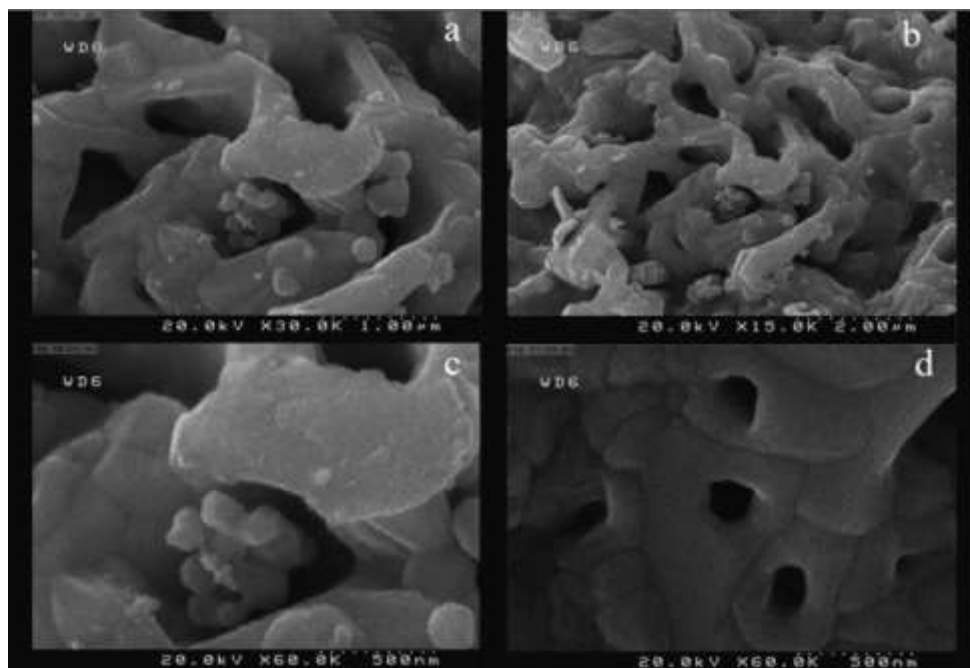


Fig. 5. FESEM images of spinel Co_3O_4

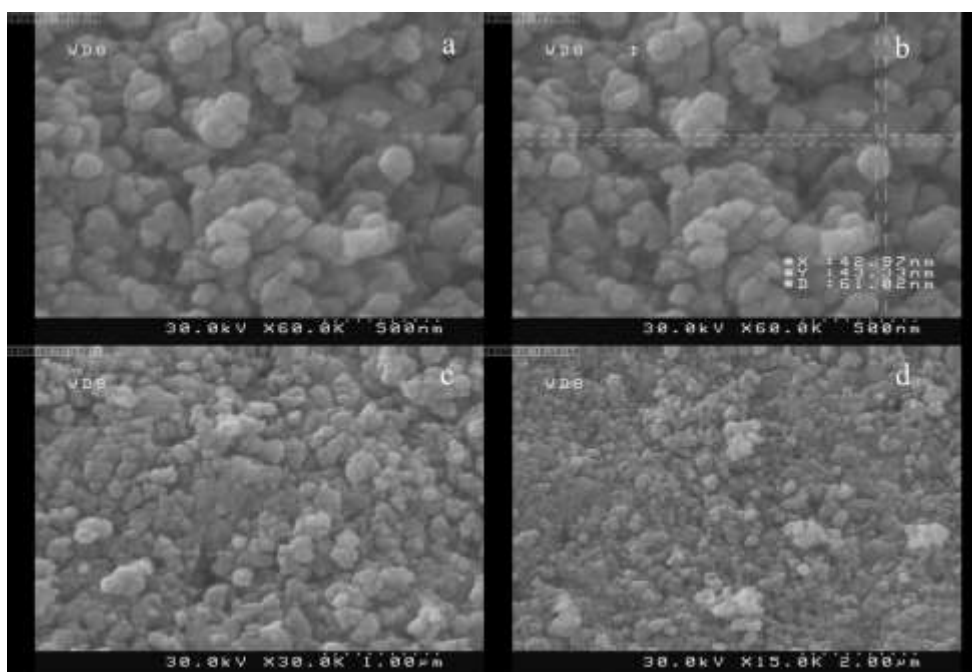


Fig. 6. FESEM images of $\text{Co}_{3-x}\text{Nd}_x\text{O}_4$ where $x = 0.01$ mmol.

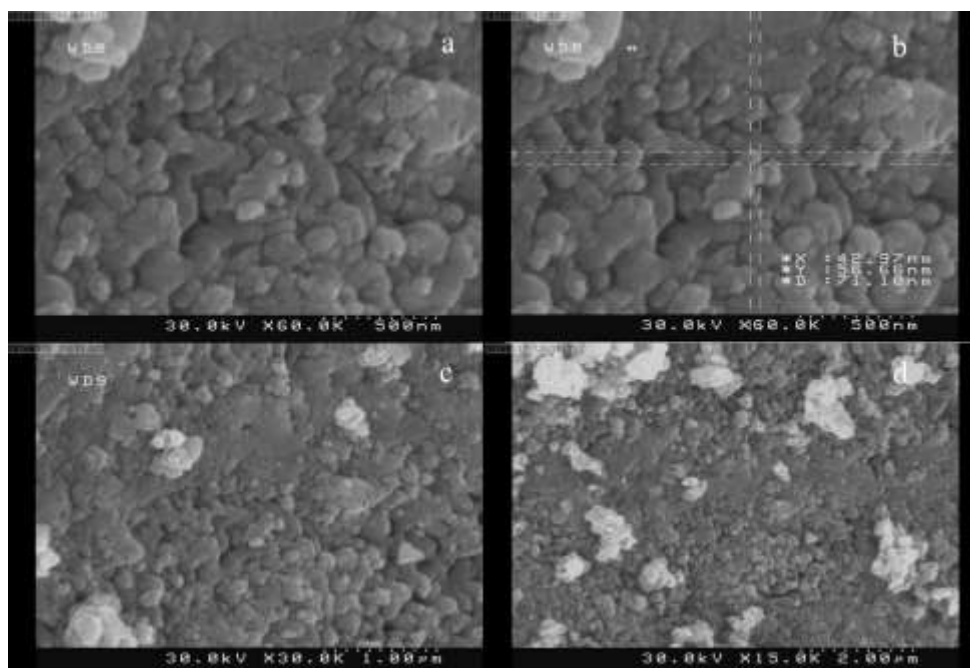
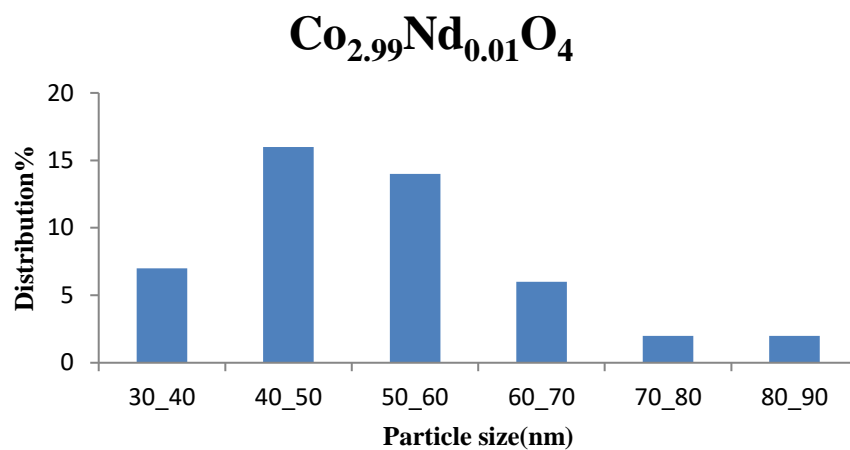


Fig. 7. FESEM images of $\text{Co}_{3-x}\text{Nd}_x\text{O}_4$ where $x = 0.03$ mmol.

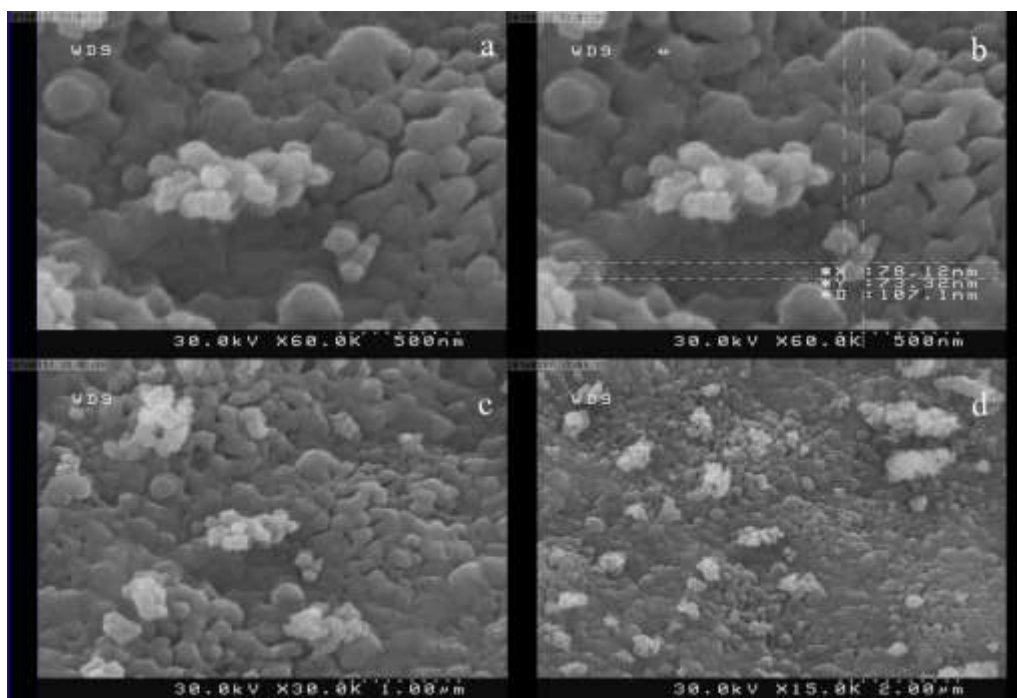
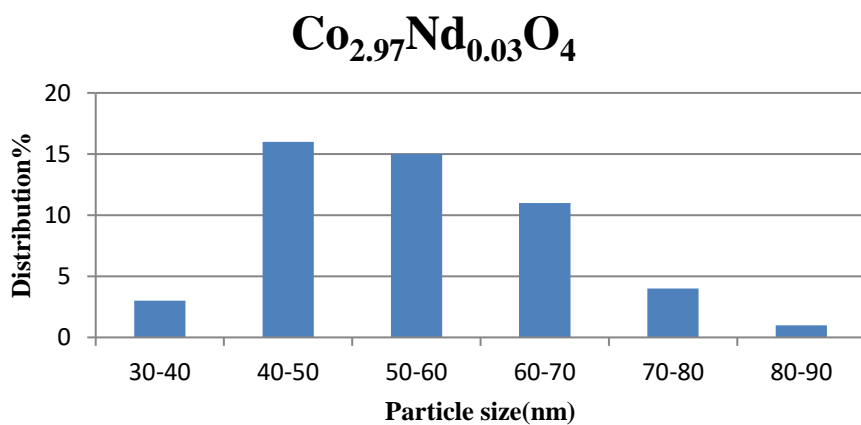


Fig. 8. FESEM images of $\text{Co}_{3-x}\text{Nd}_x\text{O}_4$ where $x = 0.05\text{mmol}$.

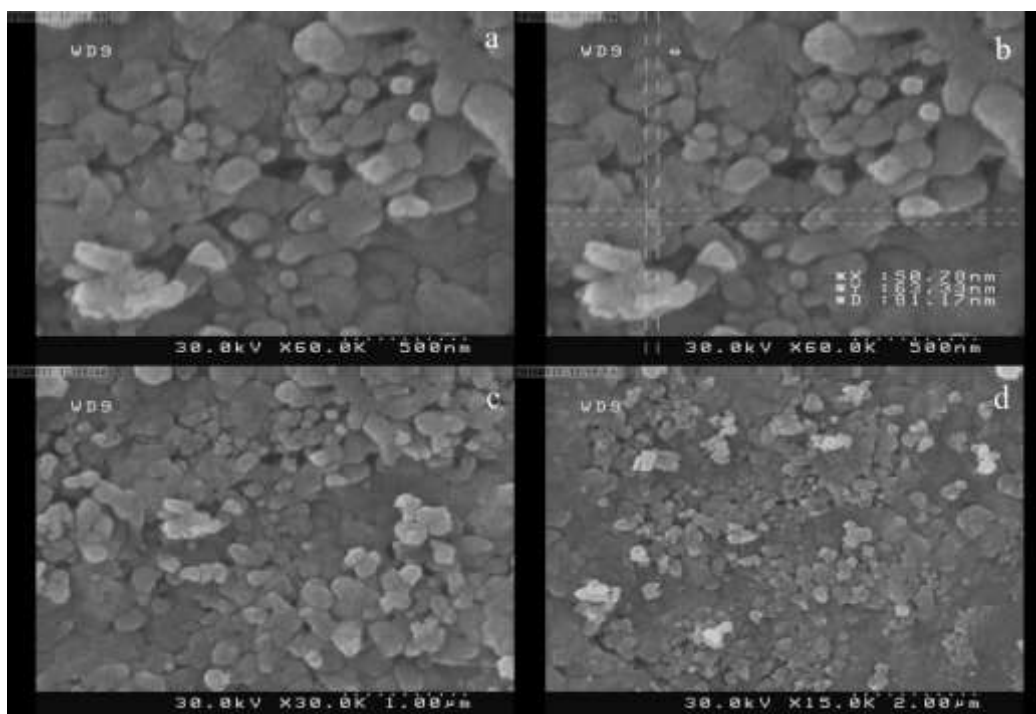
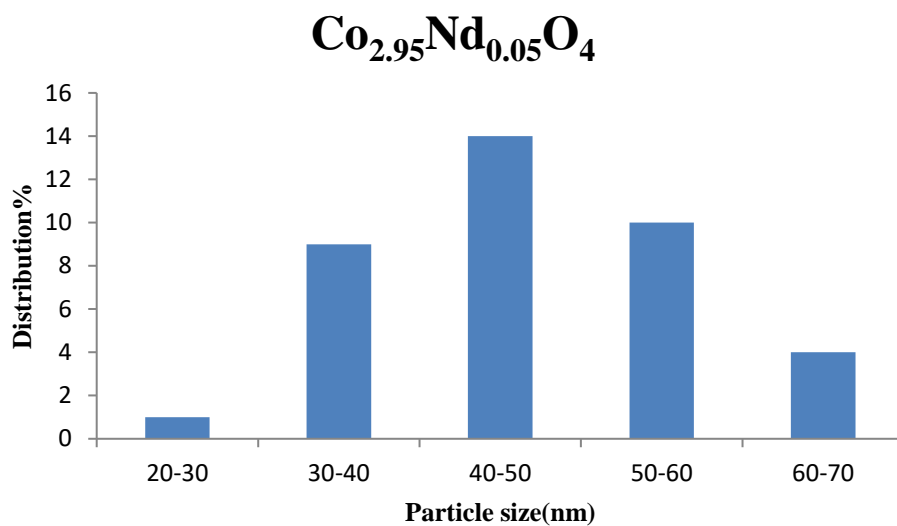


Fig. 9. FESEM images of $\text{Co}_{3-x}\text{Eu}_x\text{O}_4$ where $x = 0.01$ mmol.

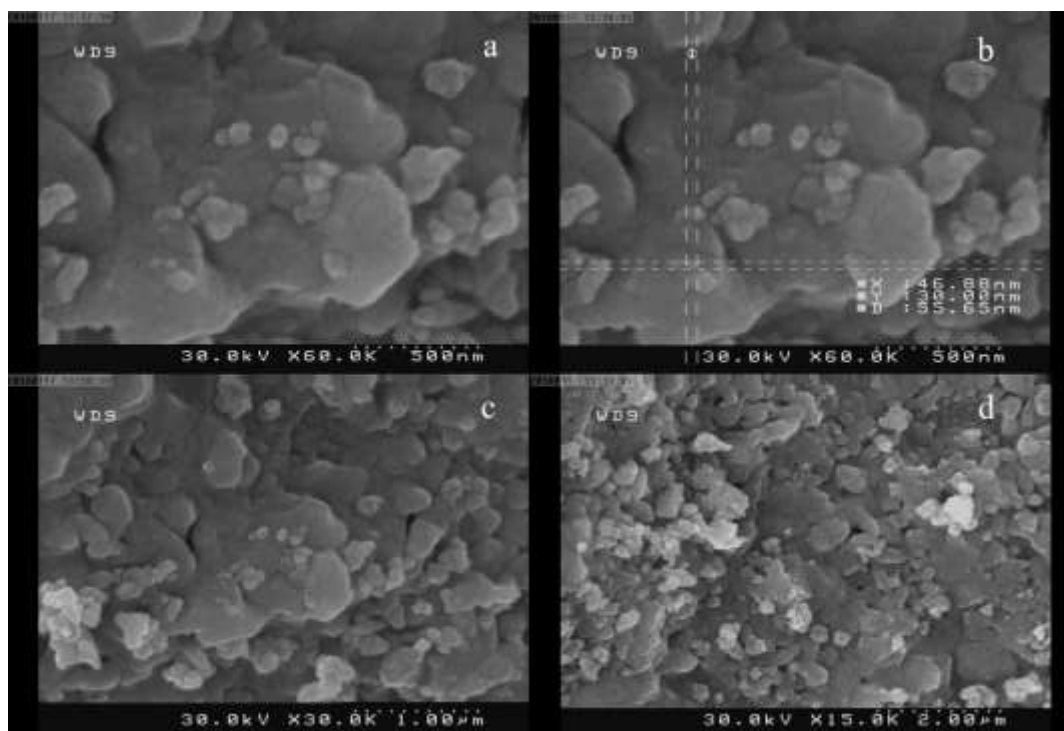
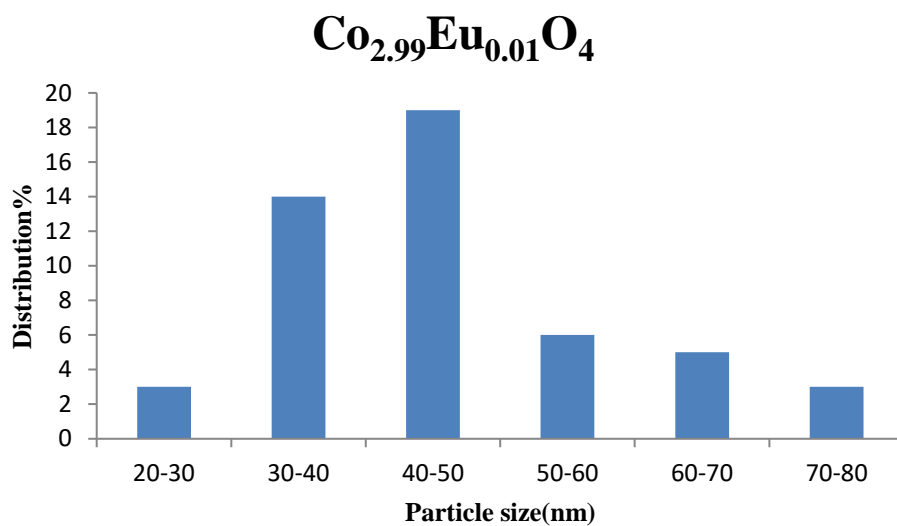


Fig. 10. FESEM images of $\text{Co}_{3-x}\text{Eu}_x\text{O}_4$ where $x = 0.03$ mmol.

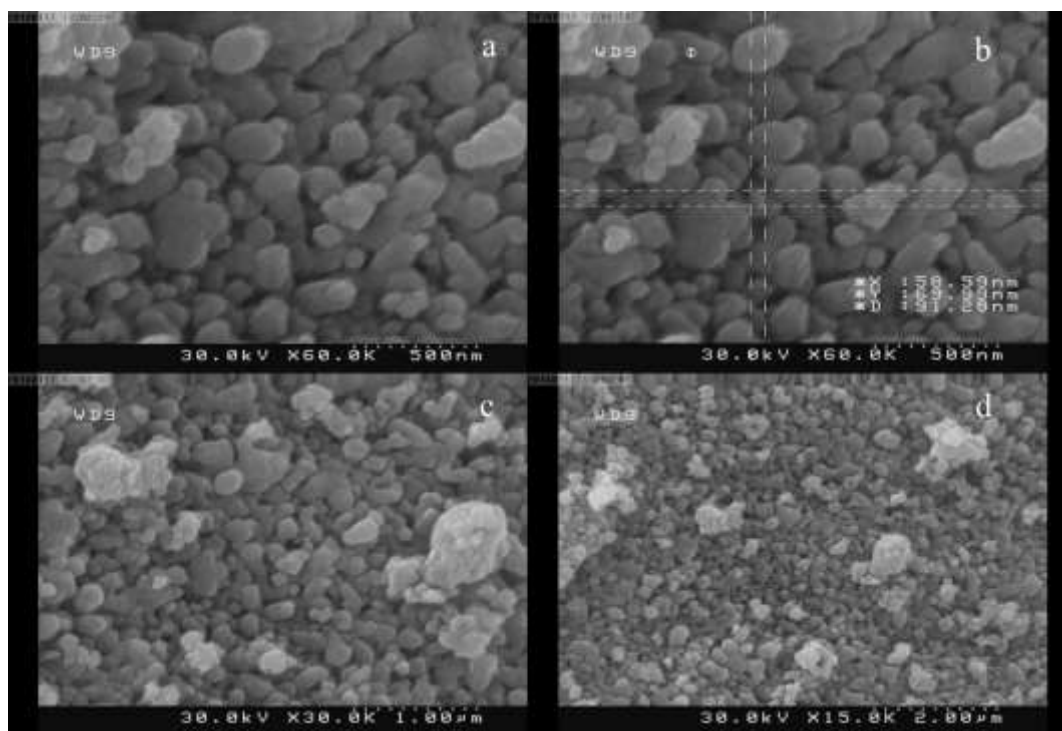
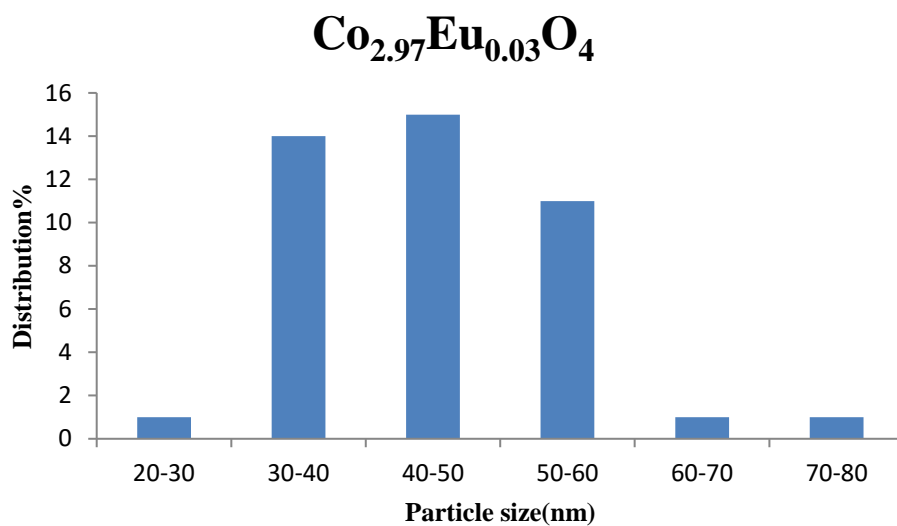
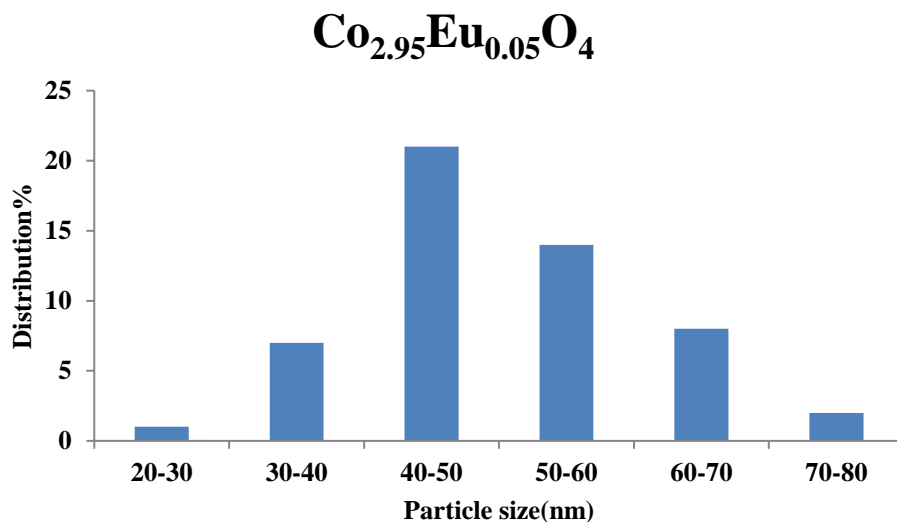


Fig. 11. FESEM images of $\text{Co}_{3-x}\text{Eu}_x\text{O}_4$ where $x = 0.05$ mmol.



2.1. Elemental analysis

Figs. 12 and 13 show the EDS elemental analysis for Co_{3-x}Nd_xO₄ and Co_{3-x}Eu_xO₄. In Fig. 12 Results show the presence of 77.29 at % Co, 3.27 at % Nd, and 19.43 at % O, for the Co_{2.97}Nd_{0.03}O₄ and Fig. 13 show the presence of 67.82 at % Co, 2.13 at % Eu, and 30.05

at % O, for the Co_{2.97}Eu_{0.03}O₄. Table 2 shows the elemental analyses data of the doped nanomaterial obtained from EDS spectra.

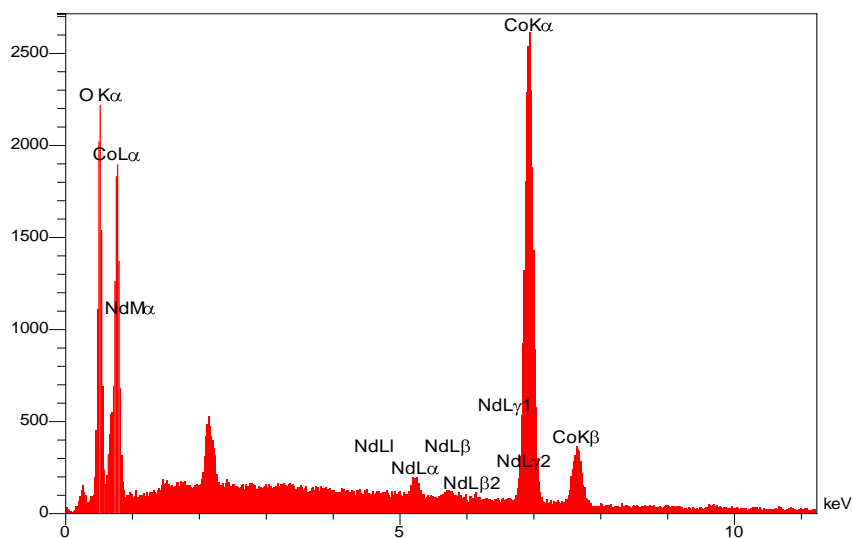


Fig. 12. EDS spectra of Co_{2.97}Nd_{0.03}O₄ nanoparticles.

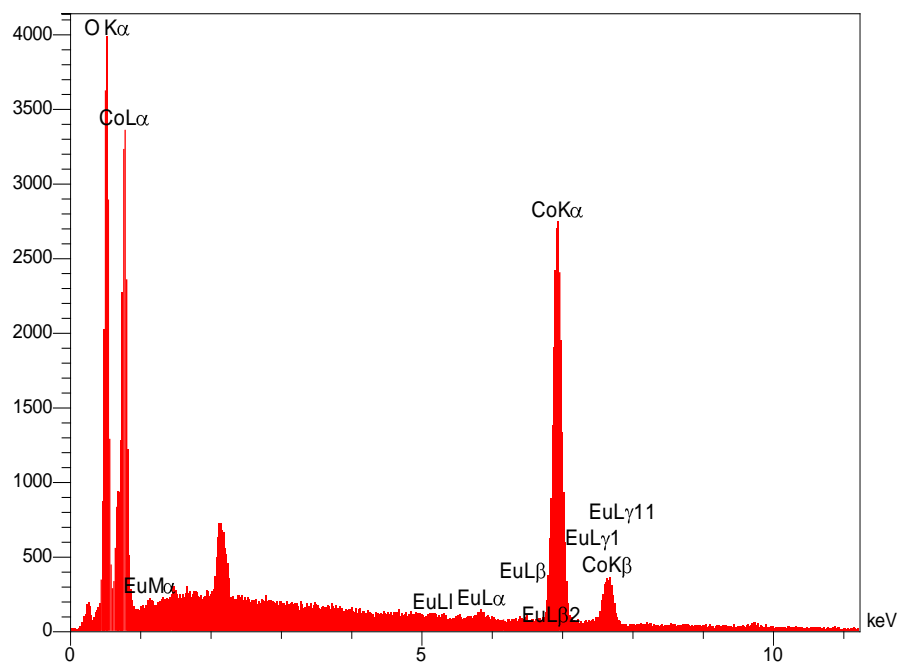


Fig. 13.EDS spectra of $\text{Co}_{2.97}\text{Eu}_{0.03}\text{O}_4$ nanoparticles.

Table 2. Elemental analyses data of the Nd^{3+} and Eu^{3+} - doped Co_3O_4 .

dopant	Normalized element analysis (wt %)
Nd^{3+}	3.27
Eu^{3+}	2.13

Fig 14 and 15 confirm MAP analysis investigation.in the EDS mapping images of the $\text{Co}_{3-x}\text{Nd}_x\text{O}_4$, Co, Nd and O signals and in image of the $\text{Co}_{3-x}\text{Eu}_x\text{O}_4$, Co, Eu and O signals are uniformly distributed across the entire structure. in The MAP analysis Fig 14 and15 further confirm that the two samples all contain Co, O and Nd,Eu elements,and no other elements are detected,which are consistent with the results of EDX.

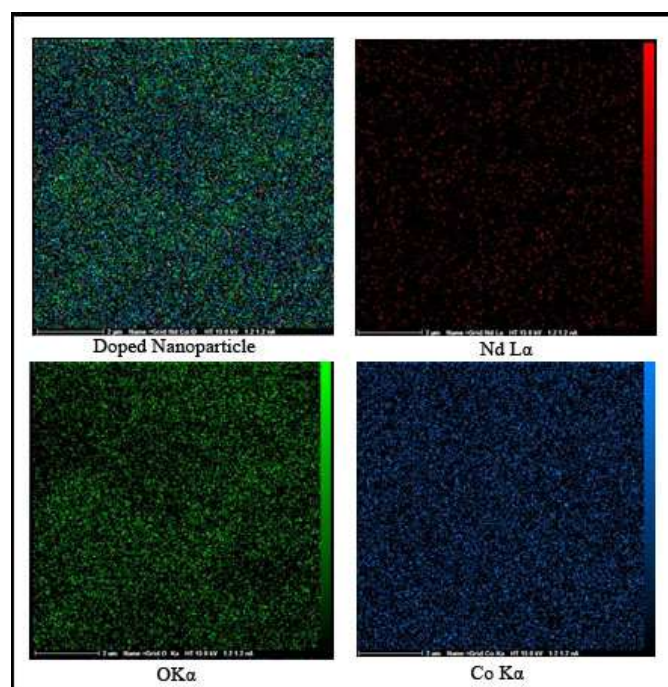


Fig. 14. Maps of Co, Nd and O distributions in sample $\text{Co}_{2.97}\text{Nd}_{0.03}\text{O}_4$.

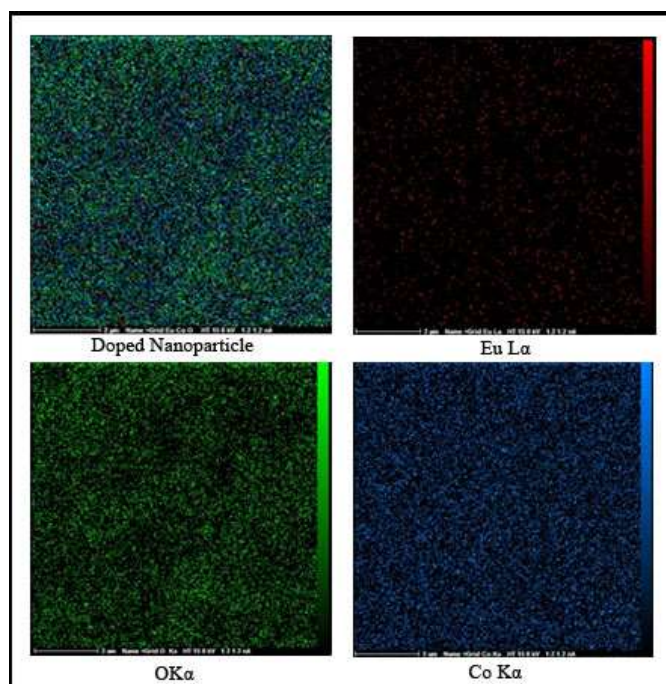


Fig. 15. Maps of Co, Eu and O distributions in sample $\text{Co}_{2.97}\text{Eu}_{0.03}\text{O}_4$

3.8. DRS

Diffuse reflectance spectroscopy (DRS) studies on Co_3O_4 , $\text{Co}_{3-x}\text{Nd}_x\text{O}_4$ and $\text{Co}_{3-x}\text{Eu}_x\text{O}_4$ nanoparticles the intercept of the straight line portion gives the band gap values. Optical band gap for the Co_3O_4 the absorption edge values for lower energy side region 2.63 and 2.9 for higher energy side region. Spectroscopy (DRS)

technique and the results showed that band gaps of $\text{Co}_{3-x}\text{Nd}_x\text{O}_4$ and $\text{Co}_{3-x}\text{Eu}_x\text{O}_4$ Nanoparticles were shifted to higher amount by increasing the Nd and Eu concentration.

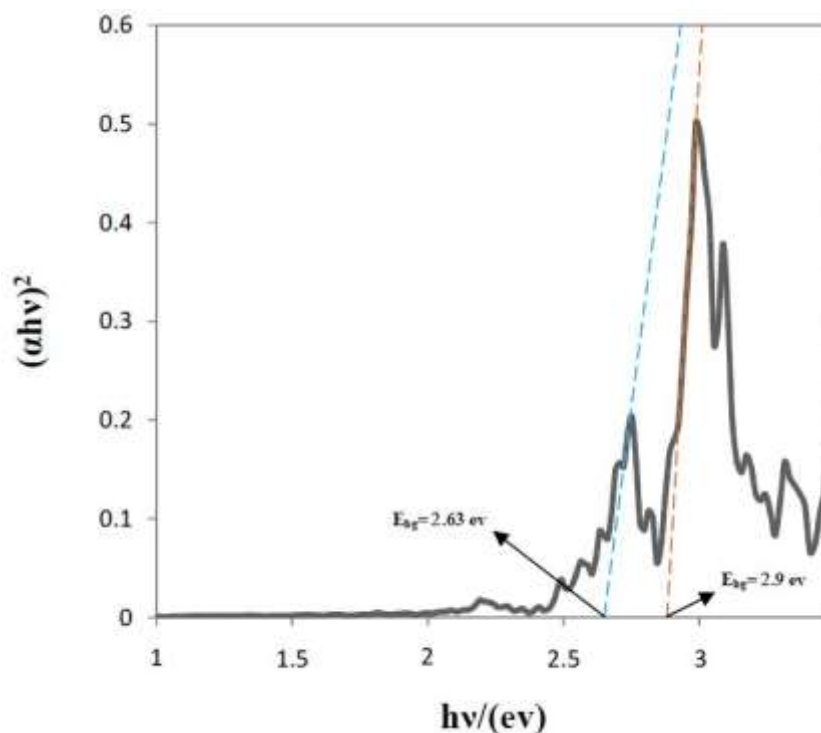


Fig. 16. diffuse reflectance spectra (DRS) of Co_3O_4 nanoparticles.

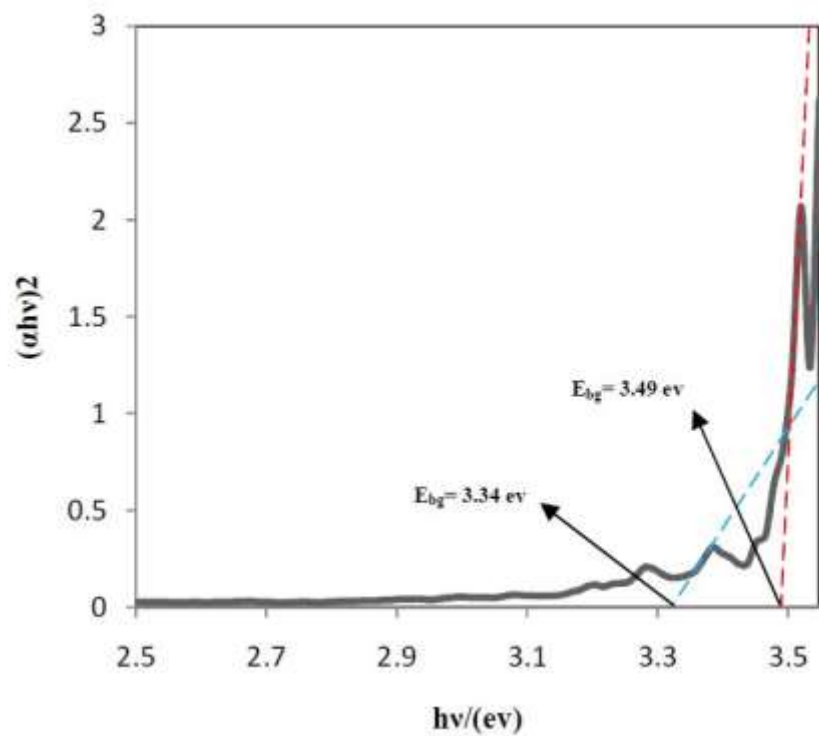


Fig. 17. diffuse reflectance spectra (DRS) of $\text{Co}_{3-x}\text{Nd}_x\text{O}_4$ nanoparticles.

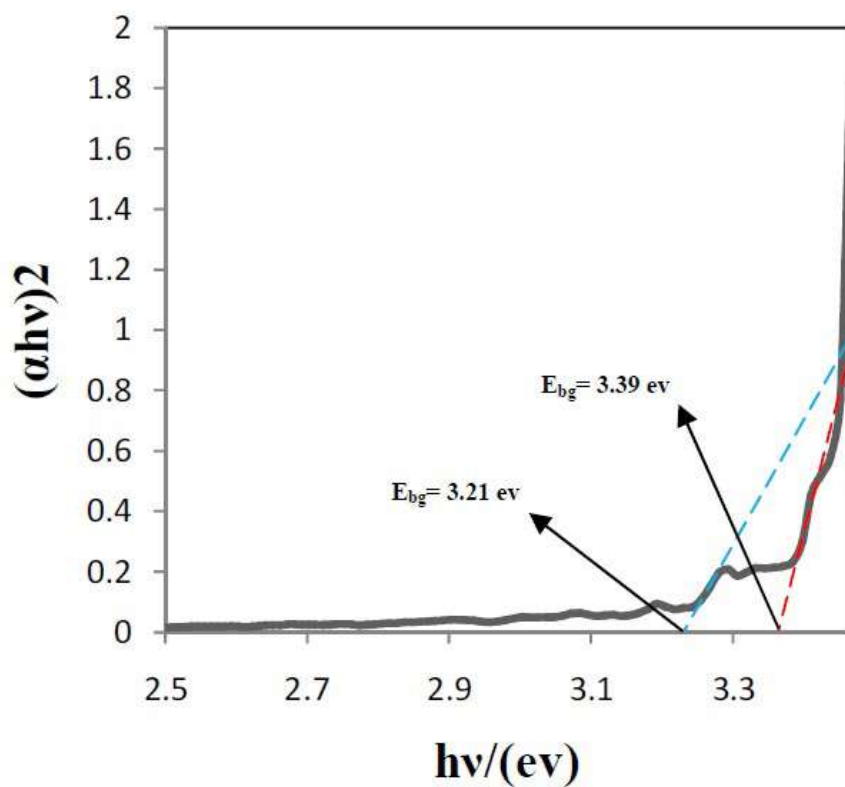


Fig. 18. diffuse reflectance spectra (DRS) of $\text{Co}_{3-x}\text{Eu}_x\text{O}_4$ nanoparticles.

3.8. Catalytic activity for oxygen evolution

Oxygen evolution reaction (OER) is one of the most important processes in various electrochemical devices. Spinal-type Co_3O_4 , an inexpensive material, has shown high activity and long term performance for OER in alkaline electrolyte. Therefore, many studies have been devoted to the improvement of the composition and structure of Co_3O_4 to increase of OER efficiency. The doping of various metals in Co_3O_4 structure is one way that is employed to increase the performance of Co_3O_4 .

The effect of eridium and neodymium doping on the electrocatalytic activity of Co_3O_4 was studied using cyclic voltammetry (CV) for the OER in alkaline media. Fig. 19 shows that the presence of eridium

efficiency increases the current of the oxygen evolution. However, neodymium has no effect on the properties of Co_3O_4 in this case. at a fixed potential of 1.1 V, current value for eridium Doping $\text{Co}_3\text{O}_4/\text{GCE}$ is 30.0 mA, which is about 10 times higher than 4.0 mA for $\text{Co}_3\text{O}_4/\text{GCE}$. Moreover, it is found that at a fixed current of 20.0 mA, the potential is 0.95 V for eridium doping $\text{Co}_3\text{O}_4/\text{GCE}$ and 1.24 V for $\text{Co}_3\text{O}_4/\text{GCE}$, i.e. the over potential is improved 0.29 V by doping eridium. The performance improvement of OER by eridium may be due to an increase in electrical conductivity.

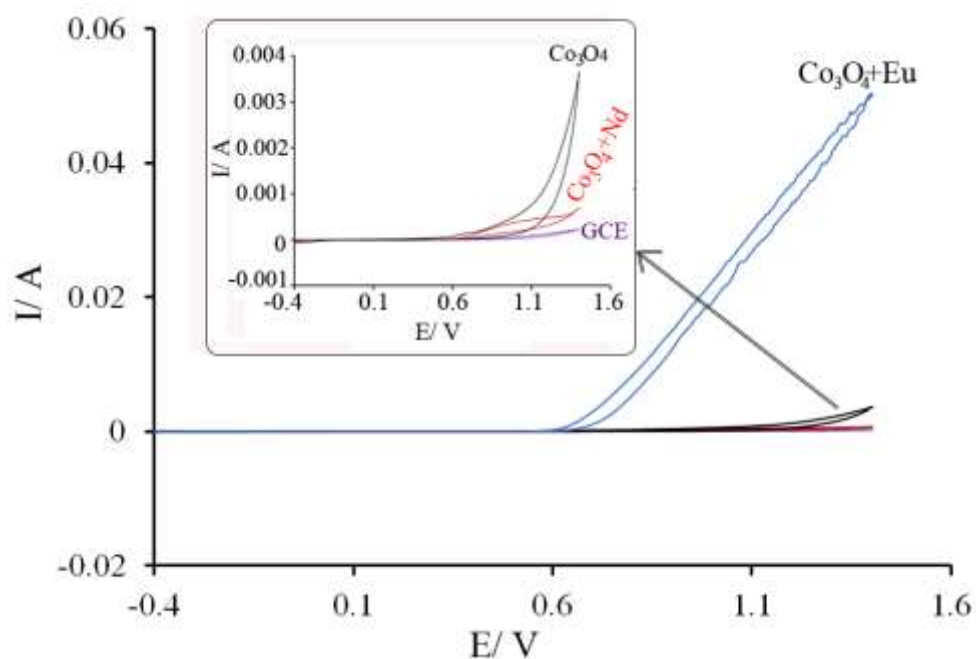


Figure 19. LSV curves on different modified electrode in $0.1 \text{ mol L}^{-1} \text{ KOH}$ with a sweep rate of 0.05 Vs^{-1}

Conclusions:

In summary, the cobalt oxide, $\text{Co}_{3-x}\text{Nd}_x\text{O}_4$ and $\text{Co}_{3-x}\text{Eu}_x\text{O}_4$ nanoparticles have been successfully synthesized by a combustion synthesis method at temperature of 700 °C for 8 h. The structure and morphology of the synthesized nanoparticles have been studied by FT-IR, XRD and FESEM analysis revealed the average particle size as 40-50 nm. The synthesis of Co_3O_4 nanoparticle with defined cubic shape, average edge length of 8 nm. SEM images showed spherical particles a few number of voids is also observed on the surface but in the $\text{Co}_{3-x}\text{Nd}_x\text{O}_4$ and $\text{Co}_{3-x}\text{Eu}_x\text{O}_4$ the particles have homogeneous structure. On the basis of the OER activity on Co_3O_4 , $\text{Co}_{3-x}\text{Nd}_x\text{O}_4$ and $\text{Co}_{3-x}\text{Eu}_x\text{O}_4$ it can be concluded that the presence of eridium exhibited a much higher oxygen evolution activity and efficiency increases the current of the oxygen evolution.

References:

- [1] K. M. Nam, Y. C. Choi, S. C. Jung, Y. I. Kim, M. R. Jo, S. H. Park, J. T. Park, *Nanoscale*. **4** (2012) 473.
- [2] Y. Qi, N. Du, H. Zhang, X. Fan, Y. Yang, D. Yang, *Nanoscale*. **4** (2012) 991.
- [3] Y. Sun, X. Hu, W. Luo, Y. Huang, *J. Mater. Chem.* **22** (2012) 13826.
- [4] L. Sun, H. Li, L. Ren, C. Hu, *Solid State Sci.* **11** (2009) 108.
- [5] N. A. Barakat, M. S. Khil, F. A. Sheikh, H. Y. Kim, *J. Phys. Chem. C* **112** (2008) 12225.
- [6] M. Salavati-Niasari, N. Mir, F. Davar, *J. Phys. Chem. Solids*. **70** (2009) 847.
- [7] T. Mousavand, T. Naka, K. Sato, S. Ohara, M. Umetsu, S. Takami, T. Adschiri, *Phys. Rev. B* **79** (2009) 144411.
- [8] T. He, D. Chen, X. Jiao, Y. Wang, *Adv. Mater.* **18** (2006) 1078.
- [9] J. Park, X. Shen, G. Wang, *Sens. Actuators B Chem.* **136** (2009) 494.
- [10] D. Y. Kim, S. H. Ju, H. Y. Koo, S. K. Hong, Y. C. Kang, *J. Alloys Compd.* **417** (2006) 254.
- [11] Y. Xuan, R. Liu, Y. Q. Jia, *Mater. Chem. Phys.* **53** (1998) 256.
- [12] N. N. Binitha, P. V. Suraja, Z. Yaakob, M. R. Resmi, P. P. Silija, *J. sol-gel sci.tech.* **53** (2010) 466.
- [13] Y. Ni, X. Ge, Z. Zhang, H. Liu, Z. Zhu, Q. Ye, *Mater. Res. Bull.* **36** (2001) 2383.
- [14] Y. Jiang, Y. Wu, B. Xie, Y. Xie, Y. Qian, *Mater. Chem. Phys.* **74** (2002) 234.
- [15] H. Shao, Y. Huang, H. Lee, Y. J. Suh, C. O. Kim, *Curr. Appl. Phys.* **6** (2006) e195.
- [16] R. Garavaglia, C. M. Mari, S. Trasatti, *Surf. technology*. **23** (1984) 41.
- [17] T. N. Ramesh, *J. Solid State Chem.* **183** (2010) 1433.
- [18] Q. Yuanchun, Z. Yanbao, W. Zhishen, *Mater. Chem. Phys.* **110** (2008) 457.
- [19] G. Laugel, J. Arichi, H. Guerba, M. Moliere, A. Kiennemann, F. Garin, B. Louis, *Catal. Lett.* **125** (2008) 14.
- [20] Y. Qu, D. J. Masiel, N. N. Cheng, A. M. Sutherland, J. D. Carter, N. D. Browning, T. Guo, *J. Colloid. Interface Sci.* **321** (2008) 251.
- [21] R. N. Singh, J. F. Koenig, G. Poillerat, P. Chartier, *J. electroanal. chem. interfacial electrochem.* **314** (1991) 241.
- [22] C. Cantalini, M. Post, D. Buso, M. Guglielmi, A. Martucci, *Sens. Actuators B Chem.* **108** (2005) 184.
- [23] W. Y. Li, L. N. Xu, J. Chen, *Adv. Funct. Mater.* **15** (2005) 851.
- [24] H. Kim, D. W. Park, H. C. Woo, J. S. Chung, *Applied Catalysis B: Environmental* **19** (1998) 233.

- [25] W. Y. Li, L. N. Xu, J. Chen, *Adv. Funct. Mater.* **15** (2005) 851.
- [26] T. Sugimoto, E. Matijević, *J. Inorg. Nucl. Chem.* **41** (1979) 165.
- [27] P. L. S. G. Poizot, S. Laruelle, S. Grugeon, L. Dupont, J. M. Tarascon, *Nature* **407** (2000) 496.
- [28] Y. Shan, L. Gao, *Mater. Chem. Phys.* **103** (2007) 206.
- [29] B. Wang, Y. Wang, J. Park, H. Ahn, G. Wang, *J. Alloys Compd.* **509** (2011) 7778.
- [30] T. Maruyama, S. Arai, *J. Electrochem. Soc.* **143** (1996) 1383.
- [31] Q. Yuanchun, Z. Yanbao, W. Zhishen, *Mater. Chem. Phys.* **110** (2008) 457.
- [32] S. Noguchi, M. Mizuhashi, *Thin Solid Films* **77** (1981) 99.
- [33] S. Lian, E. Wang, L. Gao, L. Xu, *Mater. Lett.* **61** (2007) 3893.
- [34] Y. Wang, C. M. Yang, W. Schmidt, B. Spliethoff, E. Bill, F. Schüth, *Adv. Mater.* **17** (2005) 53.
- [35] C. Liu, B. Zou, A. J. Rondinone, Z. J. Zhang, *J. Am. Chem. Soc.* **123** (2001) 4344.
- [36] M. H. Huang, Y. Wu, H. Feick, N. Tran, E. Weber, P. Yang, *Adv. Mat.* **13** (2001) 113.
- [37] B. Kim, S. L. Tripp, A. Wei, *J. Am. Chem. Soc.* **123** (2001) 7955.
- [38] B. Liu, H. C. Zeng, *J. American Chem. Soc.* **126** (2004) 8124.
- [39] J. J. Teo, Y. Chang, H. C. Zeng, *Langmuir* **22** (2006) 7369.
- [40] W. E. Spear, D. S. Tannhauser, *Physical Review B* **7** (1973) 831.
- [41] H. K. Lin, H. C. Chiu, H. C. Tsai, S. H. Chien, C. B. Wang, *Catal. Lett.* **88** (2003) 169.
- [42] Gadsden, J. A. *Infrared spectra of minerals and related inorganic compounds.* Butterworths, 1975.
- [43] Y. Chen, Y. Zhang, S. Fu, *Mater. Lett.* **61** (2007) 701.
- [44] T. Ozkaya, A. Baykal, M. S. Toprak, Y. Koseoğlu, Z. Durmuş, *J. Magn. Magn. Mater.* **321** (2009) 2145.
- [45] K. T. Wong, J. M. Lehn, S. M. Peng, G. H. Lee, *Chem Communications.* **22** (2000) 2259.
- [46] J. A. Ramsden, W. Weng, A. M. Arif, J. A. Gladysz, *J. Am. Chem. Soc.* **114** (1992) 5890.
- [47] W. Weng, J. A. Ramsden, A. M. Arif, J. A. Gladysz, *J. Am. Chem. Soc.* **115** (1993) 3824.
- [48] N. Le Narvor, L. Toupet, C. Lapinte, *J. Am. Chem. Soc.* **117** (1995) 7129.